

Supporting Information

Nanorattles with tailored electric field enhancement

Max J. Schnepf,^{a,°} Martin Mayer,^{a,b,°} Christian Kuttner,^{a,b} Moritz Tebbe,^c Daniel Wolf,^d Martin Dulle,^e
Thomas Altantzis,^f Petr Formanek,^a Stephan Förster,^e Sara Bals,^f Tobias A.F. König,^{a,b,*} and Andreas Fery^{a,b,g,*}

[°] contributed equally

^aLeibniz-Institut für Polymerforschung Dresden e.V., Institute of Physical Chemistry and Polymer Physics,
Hohe Str. 6, 01069 Dresden, Germany

^bCluster of Excellence Center for Advancing Electronics Dresden (cfaed), Technische Universität Dresden,
01062 Dresden, Germany

^cPhysical Chemistry II, University of Bayreuth, Universitätsstr. 30, 95440 Bayreuth, Germany; current address:
Department of Chemistry, University of Toronto, 80 St. George Street, Toronto, M5S 3A6, Ontario, Canada

^dHelmholtz-Zentrum Dresden-Rossendorf, Bautzner Landstraße 400, 01328 Dresden, Germany

^ePhysical Chemistry I, University of Bayreuth, Universitätsstr. 30, 95440 Bayreuth, Germany

^fEMAT, University of Antwerp, Groenenborgerlaan 171, 2020 Antwerp, Belgium

^gPhysical Chemistry of Polymeric Materials, Technische Universität Dresden, Hohe Str. 6, 01069 Dresden,
Germany

*Corresponding e-mail: A.F.: fery@ipfdd.de, T.A.F.K.: koenig@ipfdd.de

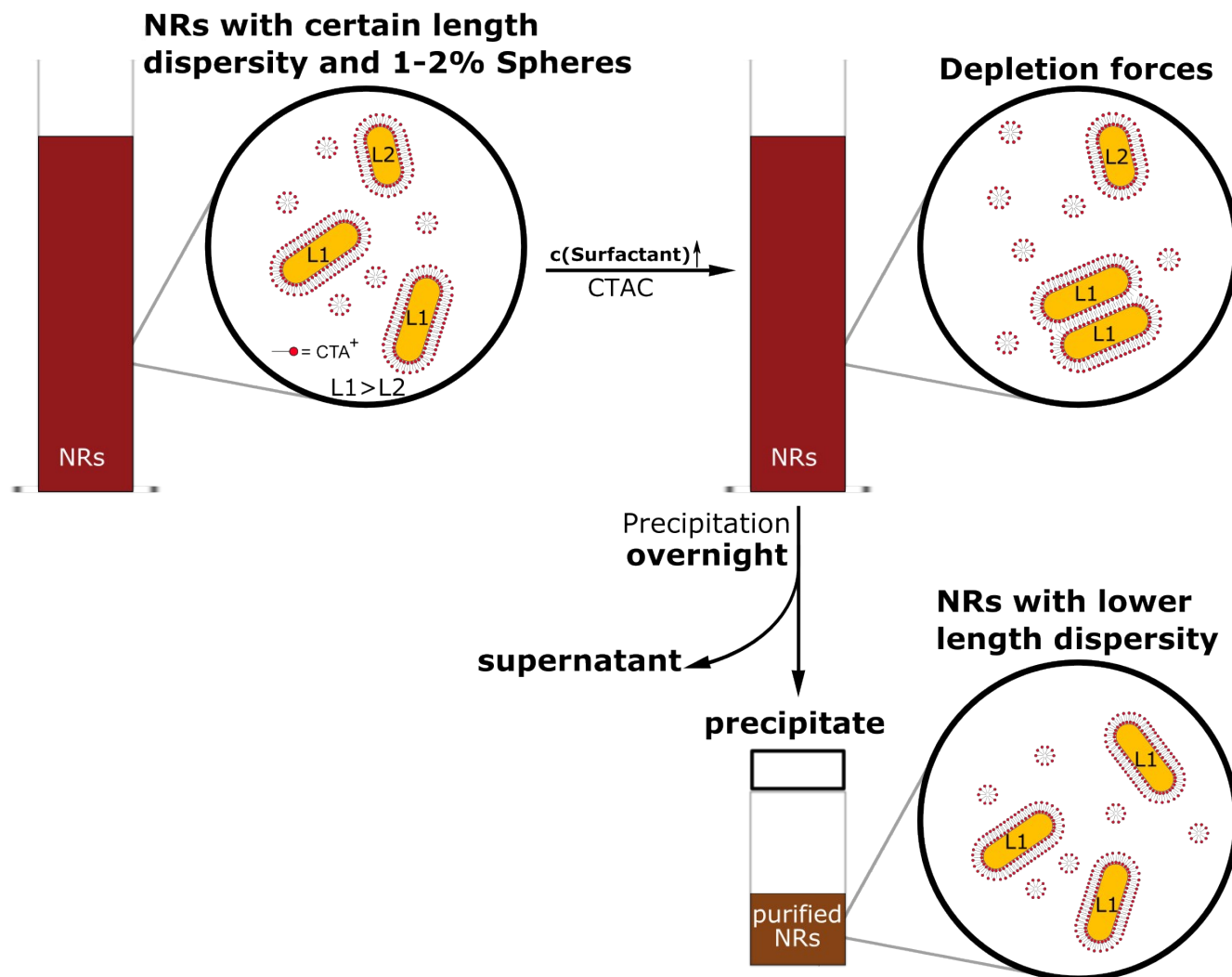


Figure S1: Schematic explanation of the depletion-forced purification step to reduce length-dispersity of the gold nanorod dispersion.

During the purification of the gold nanorods to reduce length dispersity, surfactant concentration is increased until the gold nanorods offering the most interaction area (the longest rods in the dispersion) start forming reversible flocculates and sediment. The driving force here is the entropy gain of the micelles situated between the aggregate forming gold nanorods, as well as the entropy gain of the surfactant molecules released upon flocculation. In order to fully reverse the controlled flocculation, the surfactant concentration has to be lowered, e.g. by addition of water to the sediment. As surfactant inducing the depletion forces CTAC (cetyltrimethylammonium chloride) was selected due to the seamless compatibility with CTAB (cetyltrimethylammonium bromide) in combination with a Krafft temperature below room temperature. Furthermore, a ligand exchange to CTAC is necessary for the next synthesis step (silver overgrowth). In Figure S2 results from the purification of the gold nanorods used for further silver overgrowth is shown.

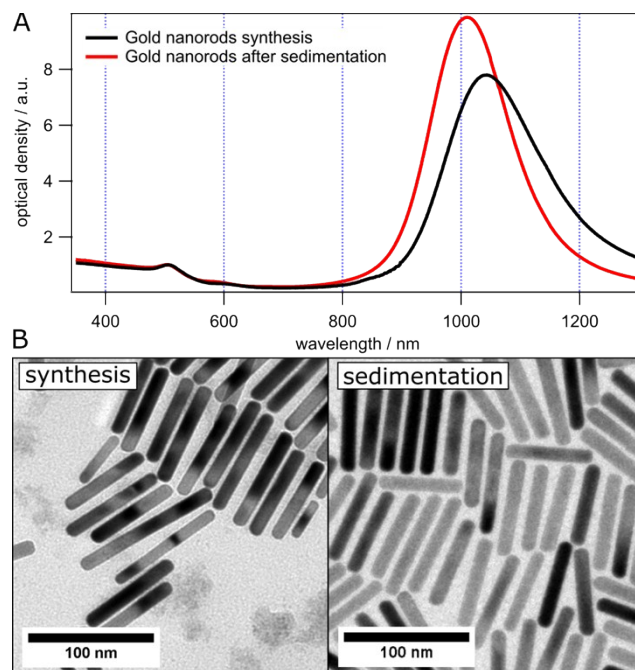


Figure S2: UV-vis extinction spectra of the gold nanorod solutions before (**black**) and after (**red**) the purification utilizing depletion forces (**A**), as well as, TEM images of the respective dispersions (**B**).

SAXS Characterization and Three-Dimensional Modeling

Nanorod model: The dimensions of the nanorod core could be accurately fitted by the simple analytical model (integrated into the *SasView* application, <http://www.sasview.org>) of a homogenous cylinder (**Fig. 2** and **Table S1**). The ligand corona of CTAC was not considered in the analysis as it exhibits a negligible scattering contrast compared to gold.

For the complex structure of the cuboid and nanorattles, the SAXS scattering curves were fitted by a three-dimensional approach over the complete (experimentally measured) q -range.¹ For this purpose, the nanoparticles were emulated by three-dimensional models consisting of randomly distributed scattering centers. Each morphology was described by a set of characteristic parameters (see **Table S1**):

Cuboid model: The cuboidal morphology of Au/Ag core/shell particles was described by 4 independent parameters (length, dispersity in length, width, dispersity in width). The scattering contrast of Au and Ag is sufficient to discriminate between core and shell of the bimetallic colloids. This model builds on the parameters of the gold nanorod which were held constant. The thickness of the silver shell was determined by evaluation of the total width and length of the particles.

Nanorattle model: The core/frame morphology of nanorattles was described by 8 parameters (length, dispersity in length, width, dispersity in width, wall thickness, silver-to-gold ratio of the shell, percentage of diffuse scattering from inside the cavity to mimic presence of structural artifacts and residues of silver salt). This model uses the dimensions of the gold nanorod core as described above. The frame (outer shell) of the nanorattle consists of an alloy of silver and gold, which ratio was to be 1:4, in accordance to experimental data. In order to account for residues of silver chloride within the nanocavity, diffuse scattering was considered by filling 9% of the cavity volume with diffuse silver scattering centers. Within the model, the wall thickness of the frame at the tip and the side of the particle were modeled as independent parameters.

The scattering curves were calculated using the program *Debyer* (<https://github.com/wojdyr/debyer>), which uses the Debye equation:²

$$I(q) = \sum_i \sum_j f_i f_j \frac{\sin(qr_{ij})}{qr_{ij}} \quad \text{Eq. S1}$$

with q being the scattering vector, r_{ij} as the distance between scattering centers i and j , and f_i as the atomic scattering factor for the i^{th} atom, which is also a function of q – but for the sake of readability, this was omitted in the formula notation. The scattering response was normalized with respect to $I(0)$ with the experimental data.

The best fit was determined by a brute-force approach, for which, all parameter combinations of a reasonable parameter range were systematically calculated. The simulation resulted in n -dimensional maps, in which the best fit was selected by comparison with the mean square error (MSE) to the complete experimental scattering profile. The standard deviation of the results was defined as a 10% deviation of the best possible fit to the experiment (lowest MSE).

Figure S2 presents the results of the SAXS evaluation. For the sake of readability, the MSE maps were reduced to the predominated parameters: width and length of the cuboid (**A**); and width, wall size and amount of diffuse scattering in the nanocavity of the nanorattle (**B**). The black dots represent the best fits as indicated by the minimum MSE (see logarithmic color scales). The high sensitivity of the SAXS response for morphological changes is illustrated in **Figure 2C–F**. Each plot represents a cross sections of the MSE map (**C**: cuboid; **D–F**: nanorattle) showing the MSE minimum for a characteristic morphological parameter. The red lines serve as guide-to-the-eye indications of the narrow range of the MSE minimum.

Table S1: Characteristic parameters of the analyzed nanoparticle morphologies. Fitting parameters are indicated by asterisks.

Model	Nanorod	Cuboid	Nanorattle
Nanorod length / nm	68.2 ± 0.0 (*)	68.2	68.2
Nanorod width / nm	10.8 ± 0.4 (*)	10.8	10.8

Cuboid length / nm	--	72.2 ± 5.8 (*)	--
Cuboid width / nm	--	31.5 ± 1.6 (*)	--
Nanorattle length / nm	--	--	77.2 ± 3.9 (*)
Nanorattle width / nm	--	--	36.0 ± 3.6 (*)
Nanorattle wall thickness tip / nm	--	--	5.5 ± 0.5 (*)
Nanorattle wall thickness side / nm	--	--	4.5 ± 0.5 (*)
Wall composition / Ag:Au	--	--	4:1 (*)
Diffuse scattering in cavity	--	--	9% (*)

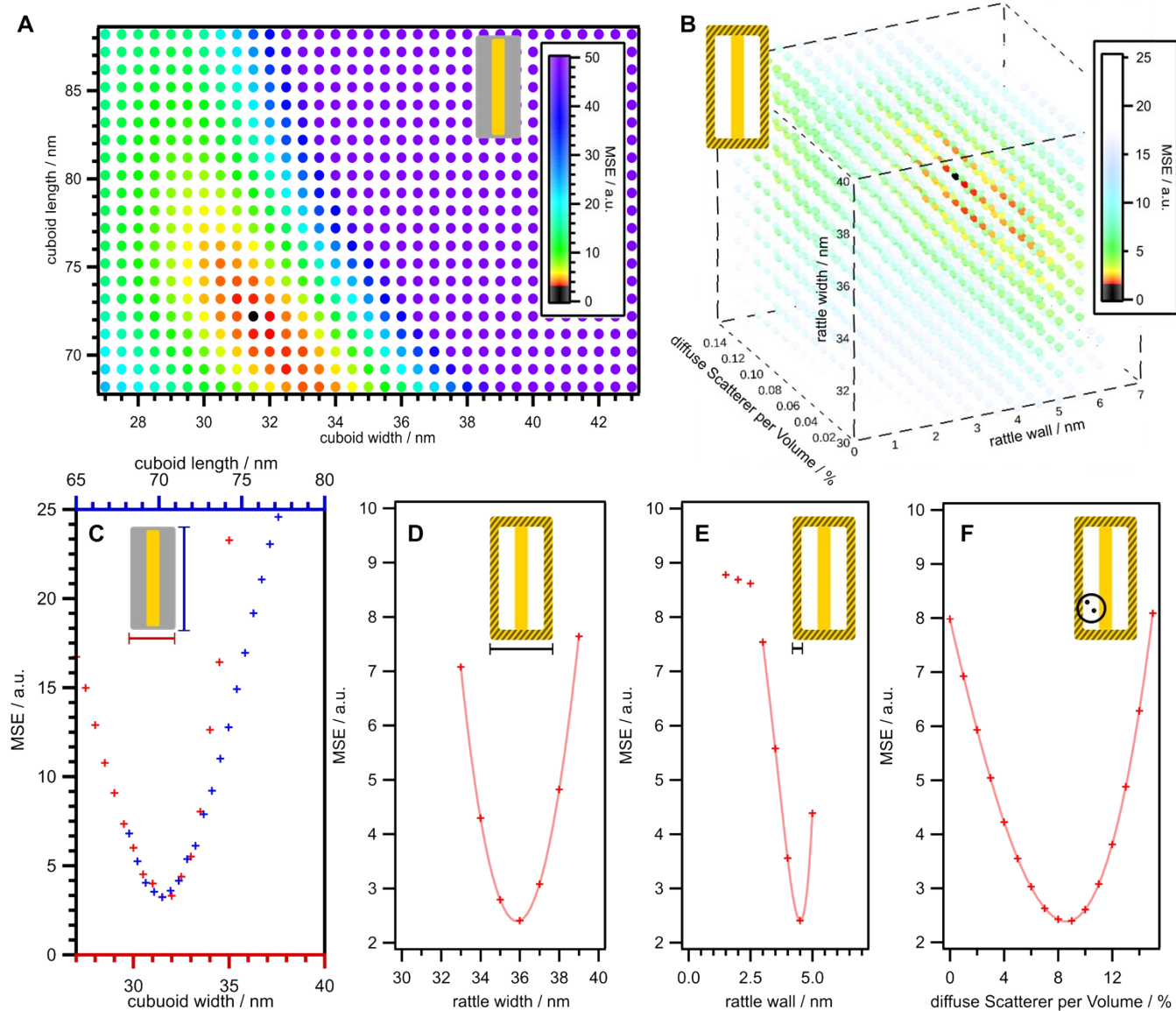


Figure S3: Evaluation of the SAXS scattering by three-dimensional modeling: MSE maps of cuboids (**A**) and nanorattles (**B**). The best-fit model, indicated by the lowest MSE, is highlighted in black color (compare **Table S1**). The nanoparticle morphology can be evaluated with very low uncertainty (<1 nm) because of the high sensitivity of

the scattering response: variation of length (**blue, top**) and width (**red, bottom**) of cuboids (**C**); variation of width (**D**), wall size (**E**), and amount of diffuse scattering from inside the nanocavity (**F**) of nanorattles.

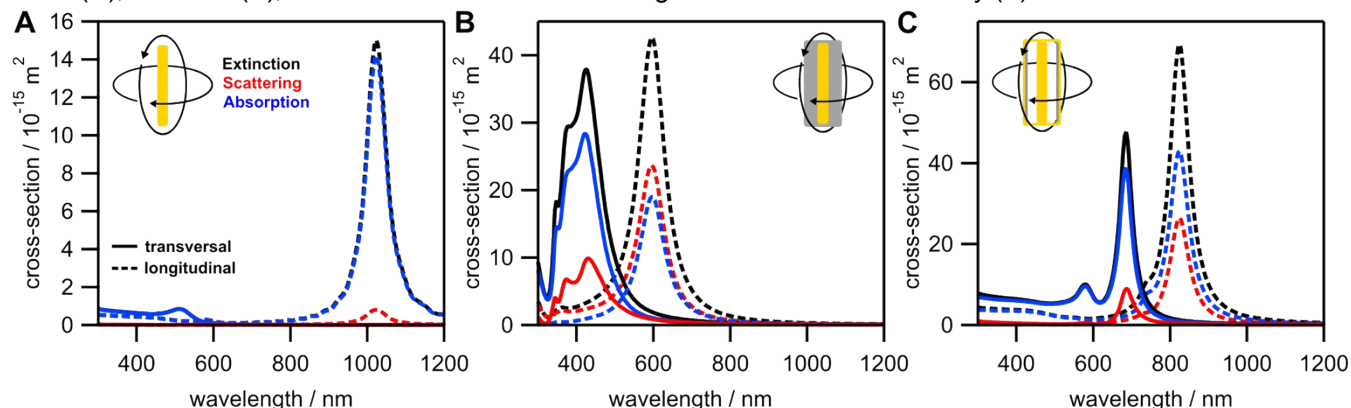


Figure S4: Simulated extinction, scattering, and absorption cross-section of nanorods (**A**), cuboids (**B**) and nanorattles (**C**) split into longitudinal (**dashed**) and transversal (**solid**) excitation. Note the appearance of *cube modes* for cuboids along longitudinal excitation. Edge rounding of plasmonic particles can be described precisely and evaluated by electromagnetic simulations using the three-dimensional SAXS model as the starting point.

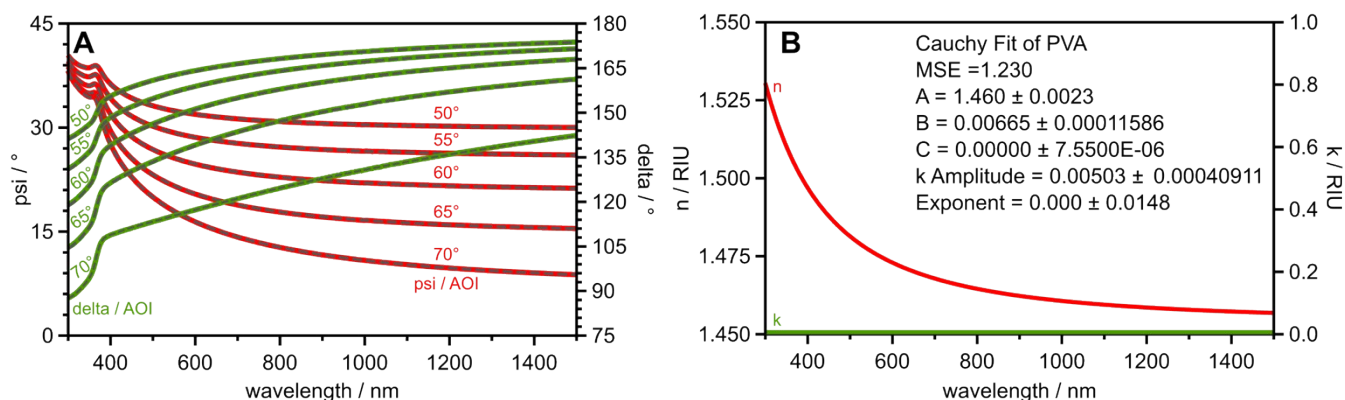


Figure S5: Variable angle spectroscopic ellipsometric data (**A**) for a PVA film spin-coated on a silicon substrate measured at incident angles of 50° to 70° in 5° steps. Psi (**green**) and Delta (**red**) were measured in the wavelength range from 300 nm to 1500 nm. The data was fitted (**gray**) using a layered isotropic model of air, PVA (Cauchy), and silicon substrate (Cauchy). See fit parameters in (**B, inset**). Optical data of the PVA film (**B**) results in a refractive index of 1.47@632 nm.

Anisotropy of in PVA embedded nanorods

The dichroic ratio DR , i.e., the ratio between the intensity of the absorption of the longitudinal mode in parallel and orthogonal excitation, can be calculated (**Eq. 2**).

$$DR = \frac{I_{parallel} - I_{orthogonal}}{I_{parallel} + I_{orthogonal}} \quad \text{Eq. S2}$$

From this polarization dependency, we obtain a dichroic ratio close to unity for the gold nanorods ($DR_{rod} = 0.97$), which corresponds to an excellent alignment of the particles within the polymer matrix.

A dichroic ratio for the latter two particle types cannot be calculated in the same way due to the overlap of the resonances frequencies.

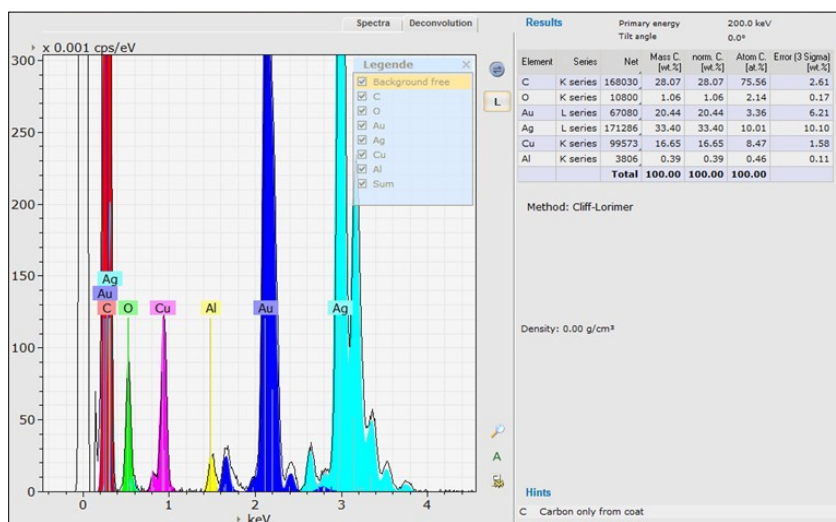


Figure S6: EDS spectrum revealing a total silver-to-gold ratio of 2.98 (weighted by atom%). Moreover, these detailed analyses reveal a silver-to-gold ratio of three (including the pure gold core, which is in good agreement with the SAXS evaluation).

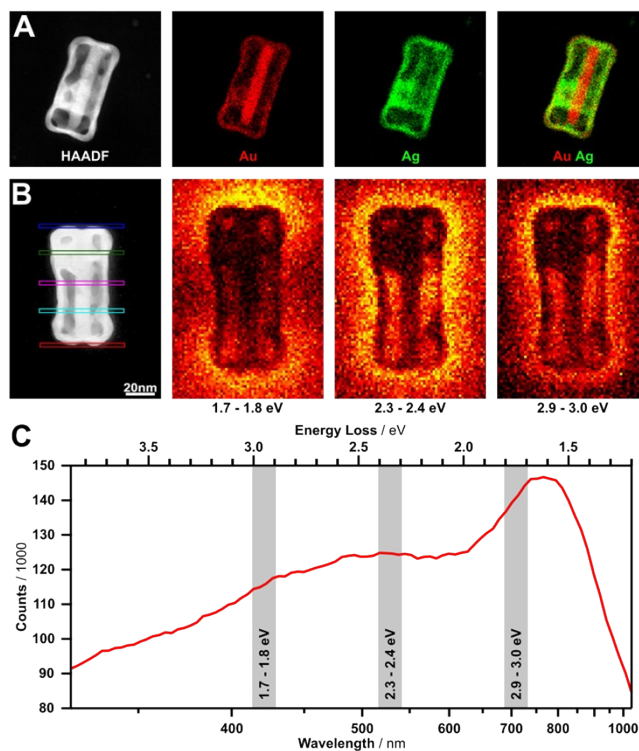


Figure S7: HAADF-STEM and EDX mappings of an alternative nanorattle (**A**). EELS trajectories and EELS mappings (**B**) of a nanorattle with an intact outer shell at distinct energies corresponding to the in (**C**) shown EELS spectra.

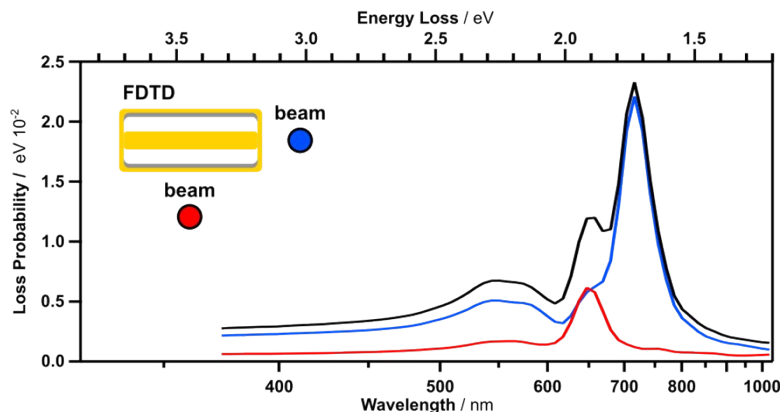


Figure S8: FDTD simulation representing the EELS experiment *via* a moving dipole source along a trajectory in *z*-direction. The simulation was performed by placing the three-dimensional morphological model of the nanorattle on a dielectric (carbon) and performing the simulations and the modeling of the setup as described by Nordlander and coworkers.³ The inset shows the resulting simulation space. The thereby performed FDTD simulations are based on a moving dipole source (representing the electron). This electron trajectory interacts with the averaged-based three-dimensional model (compare SAXS) to confirm the assignability to the far-field plasmonics of the colloidal solution.

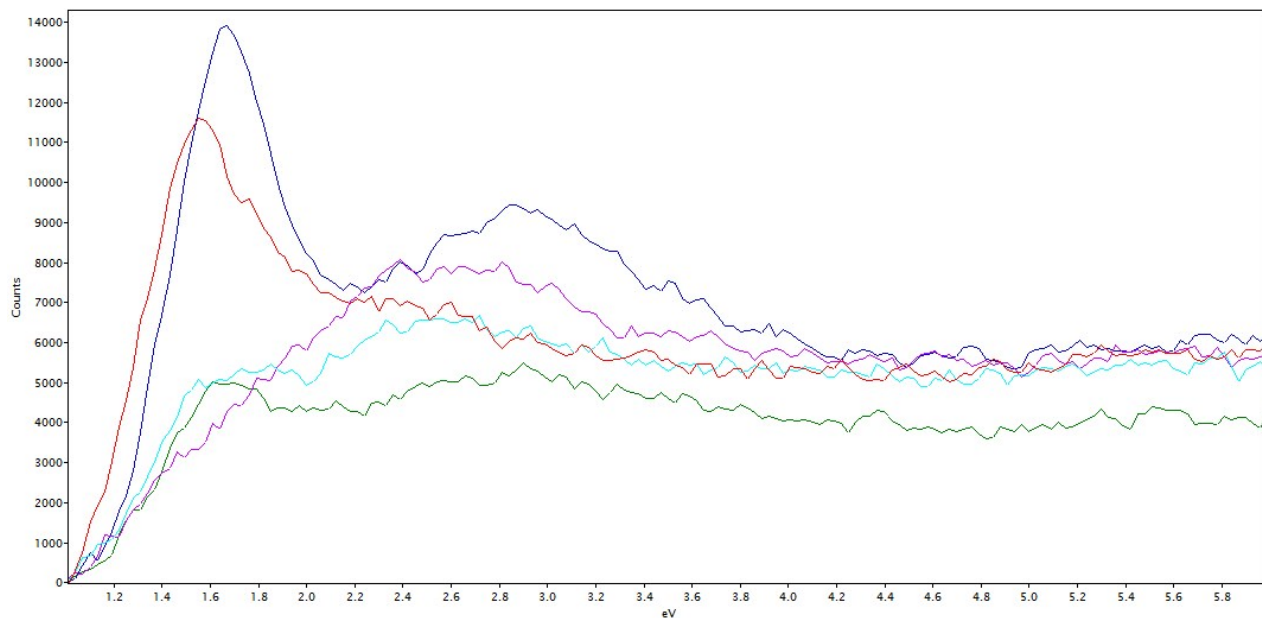


Figure S9: EDS mapping and reconstruction of the shown nanorattle. The robustness of the plasmonic properties and the advantage of the averaging in the colloidal dispersion was investigated analyzing an oxygen-influence distorted nanorattle. Even in this case, the remaining parts of the cavity are capable to form a capacitor as indicated by the distinct plasmonic field enhancement. EELS mappings and spectra (A) of the individual electron beam trajectories in dependency of the position along the long axis of the same nanorattle as shown in the HAADF-STEM image (B–C). Despite the open shell, the cavity mode can still be excited resulting in electric field enhancement inside of the nanorattle. This is evidenced by the resulting spectrum, which features a comparable signature as discussed UV-vis-NIR spectra in the manuscript.

References

1. R. P. Höller, M. Dulle, S. Thomä, M. Mayer, A. M. Steiner, S. Förster, A. Fery, C. Kuttner and M. Chanana, *ACS Nano*, 2016, **10**, 5740-5750.
2. P. Debye, *Ann. Phys.*, 1915, **351**, 809-823.
3. Y. Cao, A. Manjavacas, N. Large and P. Nordlander, *ACS Photonics*, 2015, **2**, 369-375.